Stress concentration near a surface step and shear localization

S. Brochard,* P. Beauchamp, and J. Grilhé
Laboratoire de Métallurgie Physique, Unité Mixte de Recherche 6630 du CNRS, Université de Poitiers, UFR Sciences SP2MI, Téléport 2, Boulevard Pierre et Marie Curie, Boîte Postale 30179, 86962 Futuroscope Chasseneuil Cedex, France
(Received 8 July 1999; revised manuscript received 12 October 1999)

In a previous static atomistic simulation, it has been shown unambiguously that a surface step is a privileged site for dislocation nucleation. Before dislocation nucleation, an elastic shear, localized in the plane in zone with the step where nucleation will occur, is observed. The real dislocation forms when this localized shear reaches, at its maximum, the value where the crystal gets mechanically unstable. The part played by the stress concentration on the shear localization is discussed: although the stress concentration does not involve any shear in the glide planes in zone with the step, it is shown that it produces a variation of the interplanar distance, which can make shear easier. A calculation based on the Frenkel model is developed to analyze the effect of an interplanar distance variation, and the shear distribution that minimizes the strain energy is calculated. The analytical solution obtained is then compared to the results of an atomistic simulation.

I. INTRODUCTION

Plastic deformation in bulk materials proceeds by creation and multiplication of dislocations by the Frank-Read source mechanism: under the action of the stress, a segment of preexisting dislocation can multiply and form many loops at a stress level well below the theoretical strength. But in nanostructures such as thin films, whiskers, and nanograined materials, the restricted extension offered to free dislocation motion prevents this mechanism from operating. However, these materials, in which the stress can reach several GPa, are not exempt from plastic deformation and dislocations can be observed as, for instance, misfit dislocations in thin films in epitaxy.

In these nanostructures, the dislocations are generally supposed to come from the free surface of the film or the whisker.[1,2] In this case, the dislocation is submitted to a large image force, which attracts it to the surface, so that the activation energy to nucleate the dislocation is large. The models developed show that surface nucleation requires large stress concentration or surface roughness.[3–11] If the dislocation is nucleated from a surface step, the activation energy, and consequently the stress required to nucleate the dislocation, can be significantly reduced by two factors: (i) the surface energy gain if the step disappears during nucleation and (ii) the stress concentration in the neighborhood of the step.

In a static atomistic simulation[12] realized with a face-centered-cubic crystal (aluminum), it has been shown unambiguously that a surface step is a privileged site for dislocation nucleation: the sample containing a monatomic surface step is submitted to an increasing applied stress, and for a sufficient stress level, dislocations form at the step and glide on the dense planes. The examination of the strain field in the sample as the applied stress is raised up to nucleation, reveals that the plane where the glide will occur is favored well before nucleation: neighboring atomic planes are displaced in such a way that a shear whose amplitude and extension increase with the applied stress, is progressively localized on the future glide plane; the shear direction is that of the Burgers vector of the eventual dislocation. The real dislocation is observed to form when the localized shear reaches, at its maximum, the value where the crystal gets mechanically unstable. It is thus important to understand the origin of the shear localization since it is the way by which a simple surface step transforms into a real dislocation.

It may also be worth noting that in this simulation, there are two different sets of $\{111\}$ planes submitted to the same applied resolved shear stress, but the set chosen for nucleation is always that which leads to a reduction in the step height, partial or even complete. This may be related to the surface energy gain mentioned above.

The applied resolved shear stress, identical in all the dense planes, cannot by itself induce the shear localization. But the inhomogeneity brought about by the presence of the step can play a part in the appearance of the observed strain localization. Indeed, as for a crack tip, an applied stress induces near a surface step a localized stress field,[13,14] which is not homogeneous in the step region, and leads to a stress distribution different in the two sets of $\{111\}$ planes. The part played by the stress concentration in the neighborhood of the step is examined here; its possible effect on the shear localization and on the dislocation nucleation is discussed.

In Sec. II, the results of the simulation of the dislocation nucleation mentioned above[12] are briefly recalled. In Sec. III, the localized elastic shear is described and its possible origins are investigated: although the stress inhomogeneity induced by the step does not directly involve any shear in the planes in zone with the step, it is shown that the stress concentration yields to a variation of the interplanar distance, which can make shear easier. In Sec. IV, the effect on glide, of varying the interplanar distance of $\{111\}$ planes, is examined. An analysis based on the Frenkel model[15] is developed which allows an analytical calculation of the shear distribution that minimizes the strain energy when the interplanar distance is varied. This analytical solution is then compared to the results of an atomistic simulation.

II. DISLOCATION NUCLEATION FROM A SURFACE STEP

The atomistic simulation which shows dislocation nucleation from the surface step with the precursory shear con-

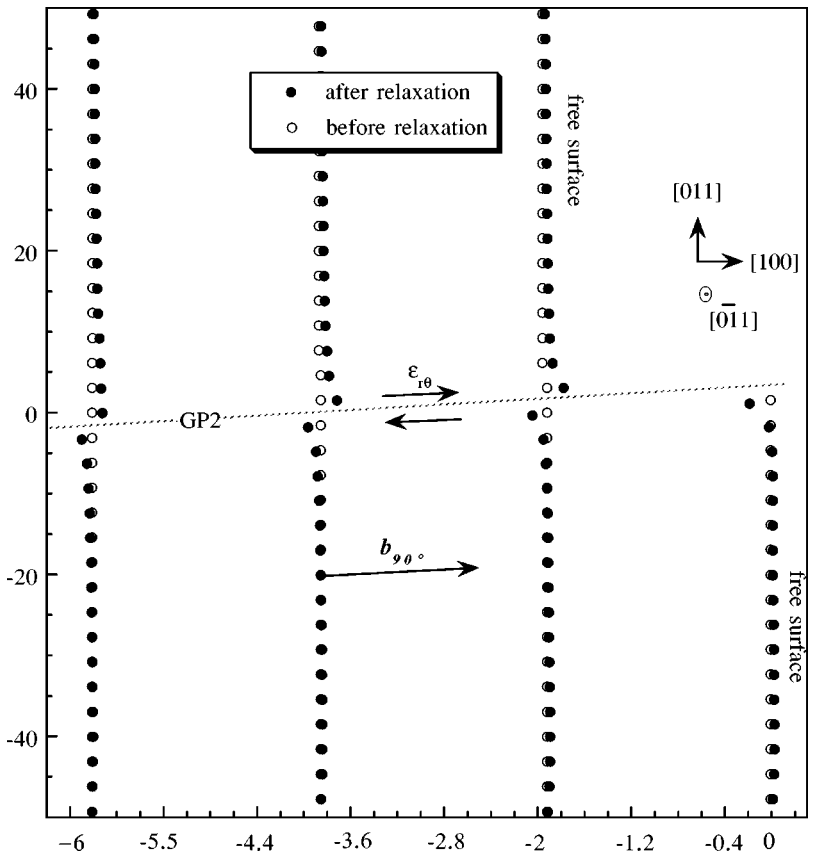

FIG. 1. Crystal structure in the step region before and after relaxation, for an applied elongation along [011] of 8.3%. The picture has been expanded along the surface normal [100]. The step line lies along [$0\bar{1}1$].

fined in the glide plane, has been reported in detail elsewhere.[12] The interatomic forces are derived from a semiempirical many-body potential for aluminum.[16] A brief description of the computational procedure and of the results follows but Refs. 12 and 16 should be consulted for more details on the geometry and the potential.

On the (100) free surface of an aluminum crystal, the monatomic step is set along a close-packed direction [$0\bar{1}1$]. The crystal remains periodic in the step direction, with the period equal to the nearest-neighbor distance. In the standard sample, the (100) surface is free and the other three sides of the computational block are kept fixed. Several stress orientations have been studied, all contained in the (100) surface. The strain is progressively increased with a characteristic step of 1%.

Consider first the results obtained with the stress axis normal to the step line (i.e., parallel to [011]): in tension, dislocations are nucleated at a strain $\bar{\varepsilon}$ of 8.4% which is definitely lower than the value calculated for the theoretical strength, equal to 15%. The dislocations are Shockley partials of pure edge character, with Burgers vector $\mathbf{b}_{90°}=a_0/6[211]$. They are nucleated in two {111} planes: GP2 in zone with the step, and GPA2 just above GP2. A test realized with a smaller computational box shows that the first event is the nucleation in GP2.

The deformation state of the crystal for applied stresses below nucleation reveals the localization of a shear strain in the plane where the first nucleation will occur. For a tensile stress axis normal to the step line, the case detailed here, this plane is GP2. For other stress orientations such as a uniaxial compression at 18° from the normal to the step line, the strain concentrates in GP1, the other plane in zone with the step, in which the first dislocation formed will glide for this orientation. This localized elastic shear strain precursor of the dislocation formation is discussed in the following sections.

III. DESCRIPTION AND ORIGIN OF THE LOCALIZED ELASTIC SHEAR

A. Description

We consider the crystal state just before dislocation nucleation, that is for an imposed elongation $\bar{\varepsilon}$ equal to 8.3% along the normal to the step line (the [011] direction). Figure 1 shows the atom positions in the step region before and after relaxation. Figure 1 is intentionally expanded along the surface normal, in order to make clear the main feature of the strain field, that is the shear in the {111} plane GP2: atoms situated on the one side of GP2 are displaced with respect to those on the other side in a direction normal to the step line and essentially parallel to GP2, that is mainly along [211].

If one refers to the polar coordinates r and θ in the ($0\bar{1}1$) plane (normal to the step line), with the origin on the outer edge of the step, the strain localized in the plane GP2 is a shear of type $\varepsilon_{r\theta}$. In this plane, $\theta\approx 35°$, and $\varepsilon_{r\theta}=(u_+ - u_-)/a$, where a is the interplanar distance and u_+ and u_- are the displacements of the atoms, respectively, above and

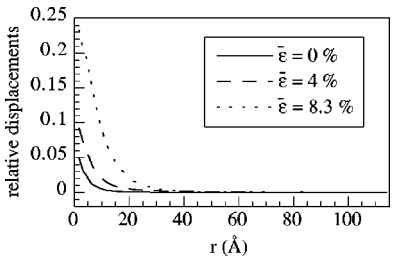

FIG. 2. Relative displacements across GP2 along the edge direction, normalized to $b_{90°}$, for 0, 4, and 8.3 % elongations along [011], versus position in the glide plane. The free surface is at $r = 0$ Å.

below the plane GP2 in the [211] direction. Note that the reference state for atomic displacements is the crystal submitted to the homogeneous strain.

The shear $\varepsilon_{r\theta}$ is illustrated in Fig. 2 where the relative displacements of atoms across GP2 after relaxation are plotted as a function of the position r, for different homogeneous applied strains. These are the relative displacements parallel to $\mathbf{b}_{90°}$, to which they are normalized ($\mathbf{b}_{90°} = a_0/6[211]$ is the Burgers vector of the 90° Shockley partial nucleated for a strain of 8.4%); the relative displacements along the step line direction are zero and very small along the normal to GP2. In Fig. 2, comparison of the curves corresponding to 4 and 8.3 % elongation shows that the localized shear increases dramatically as nucleation is approached.

Finally, in order to follow the crystal behavior as close as possible to the nucleation point, very small strain increments (0.01%) have been imposed. It is then seen that at 8.3% total strain, the localized shear reaches at its maximum, that is in the near-surface region, a value corresponding to a relative displacement between atoms equal to $\mathbf{b}_{90°}/4$. This is comparable to the state described by Rice as incipient dislocation at a crack tip,[17] although quantitatively different. This point will be further discussed in Sec. IV, in relation with the stability limit of a crystal submitted to shear.

B. Origin of the localized shear

The question here is how does the presence of the step lead, in the stressed crystal, to the shear confined in one dense plane, precursor of the dislocation nucleation?

A first approach to the calculation of the stress field in the neighborhood of a surface step in a stressed crystal can be based on the point force model: the step is regarded as a point where the external stress is not applied (Fig. 3). To check the effect of the local stresses on the formation of the observed localized shear, the following simulation has been performed: on a planar {100} surface (exempt of any step) of the fcc aluminum crystal, forces tangential to the surface plane are applied along the ⟨110⟩ dense direction. Within the point force approach, these forces produce the stress concentration due to a step in the material submitted to the homogeneous stress σ_0. Their intensity is $\sigma_0 h$ where h is the step height. After relaxation, an elastic shear of the same order of magnitude as that observed in the sample containing the step, appears in the {111} plane GP2. This shows that the elastic shear $\varepsilon_{r\theta}$ observed in the sample containing the step is essentially an effect of local stresses induced by the presence

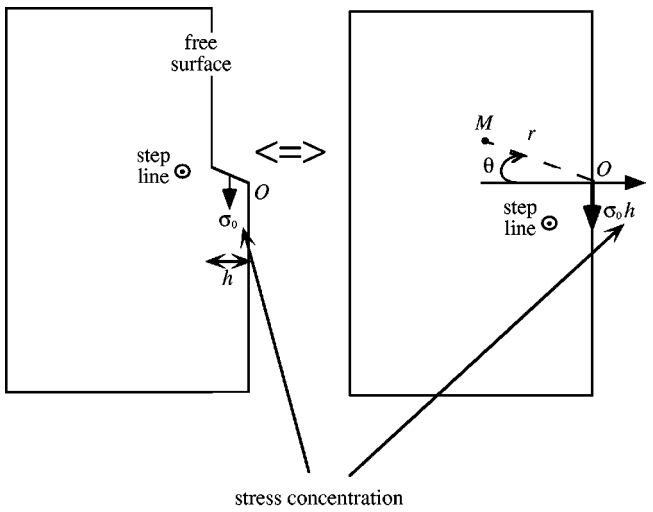

FIG. 3. Modelization of the stress field due to the step in a crystal submitted to a tensile stress.

of the step. The stress concentration is determinant in the formation of the localized shear $\varepsilon_{r\theta}$ and on the important increase of this shear.

The point force problem in an elastic isotropic continuum has received some solutions: following Boussinesq[18] and Timoshenko and Goodier,[19] the stress field due to the tangential forces is, in polar coordinates,

$$\sigma_r = -\frac{2\sigma_0 h}{\pi}\frac{\sin\theta}{r} \quad \text{and} \quad \sigma_\theta = \sigma_{r\theta} = 0, \tag{1}$$

so that the shear $\varepsilon_{r\theta} = (1/\mu)\sigma_{r\theta}$ (μ being the shear modulus of the material) is zero, contrary to the localized shear observed in GP2 in the simulation (Fig. 1). Thus, in an isotropic elastic continuum, the stress concentration in the neighborhood of the step does not act directly on the appearance of the localized shear.

In the elastic solution of the problem of tangential forces distributed along a line on the planar surface, it can be noted that, if the strain component $\varepsilon_{r\theta}$ vanishes, on the contrary the component ε_θ is not zero:

$$\varepsilon_\theta = \frac{1}{E}(\sigma_\theta - \nu\sigma_r) = \frac{\nu}{E}\frac{2\sigma_0 h}{\pi}\frac{\sin\theta}{r}, \tag{2}$$

E and ν being, respectively, the Young's modulus and the Poisson's ratio of the material. This strain component can have an effect on the localized elastic shear. Indeed, for a homogeneous traction stress, ε_θ is positive in GP2, producing an increased separation between atoms situated on each side of GP2 (Fig. 4), and then shear can become easier in this plane, as discussed for instance in the tension-shear coupling analysis made by Sun, Beltz, and Rice[20] for dislocation nucleation at the crack tip. The tests made with other stress orientations[12] confirm that the first glide event occurs in the plane in which ε_θ is positive, i.e., GP2 in traction and GP1 in compression.

The separation between {111} planes, obtained in the atomistic simulations of the crystal containing the step, is plotted in Fig. 5. The strain $\varepsilon_{\theta'}$ shown in Fig. 5 is calculated according to Eq. (3):

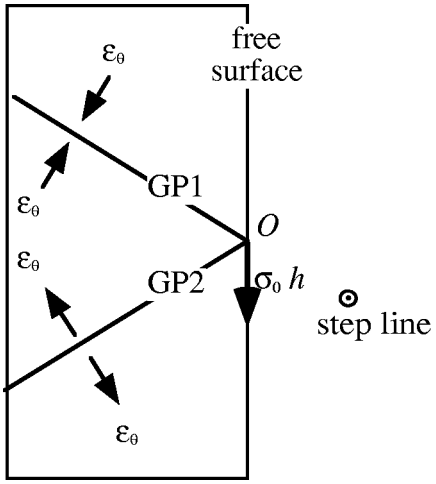

FIG. 4. Effect of stress concentration on the separation between planes.

$$\varepsilon_{\theta'}=\frac{l-l_0}{l_0}, \tag{3}$$

where l_0 is the interplanar distance before relaxation in the crystal submitted to the homogeneous strain, and l is the same quantity after relaxation. Note that the equality $\varepsilon_{\theta'}=\varepsilon_\theta$ holds in GP2 and GP1, in zone with the step, but is not quite exact in the other planes. Although the results differ from the elasticity [Eq. (2)], it is seen from Fig. 5 that $\varepsilon_{\theta'}$ is positive and large in GP2, while in the other planes $\varepsilon_{\theta'}$ remains small. The assumption of an effect of the interplanar distance on the shear localization seems then well founded. This point is discussed in detail in the following section.

IV. {111} PLANE SEPARATION EFFECT

In this section, the effect of {111} plane separation on the shear properties of these planes is investigated, in order to evaluate the part played by the strain ε_θ on the localization of the elastic shear $\varepsilon_{r\theta}$ observed before dislocation nucleation from a surface step. To examine this effect, the fcc crystal is regarded as the stacking of {111} rigid atomic planes and a modulation of the interplanar distance is imposed along the plane normal [(Ox) direction]; the sample is submitted to a shear strain of mean value $\bar{\varepsilon}$, and the local shear $\varepsilon_{xy}(x)$, which minimizes the crystal energy, is determined. Two approaches to the problem are taken: first, an analytical calculation applied to a continuum allows the determination of the local shear as a function of the imposed local elongation (variation in the interplanar distance), with the help of a variational procedure; second, an atomistic energy minimization performed on the sample constituted of rigid {111} planes, with the aluminum potential, allows the determination of the {111} planes relative position, keeping the imposed separation. The parameters entering in the analytic calculations are taken from the aluminum interatomic potential in order to make the two approaches comparable.

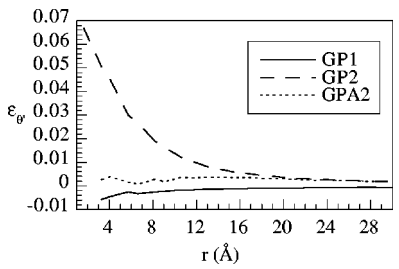

FIG. 5. Strain $\varepsilon_{\theta'}$ calculated using Eq. (3) in GP1, GP2, and GPA2, for a 4% elongation along [011], versus position in the glide planes.

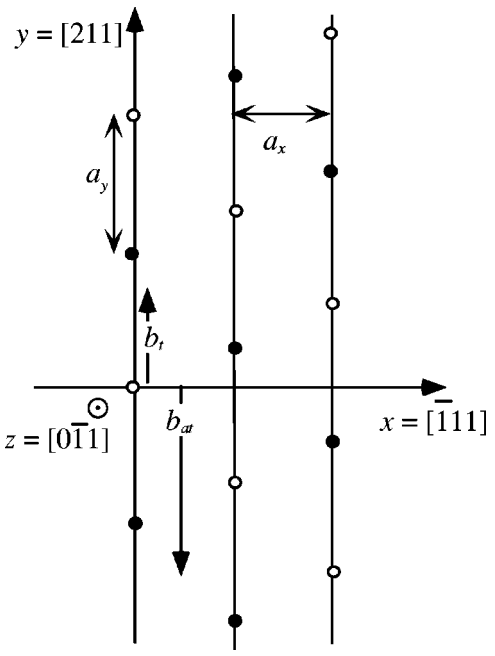

FIG. 6. Stacking of {111} planes in the chosen geometry. The full circles are atoms contained in the sheet plane, and the open circles are in the plane parallel to the sheet plane at the height $a_0 2^{1/2}/4$. $a_x=a_0/3^{1/2}$ and $a_y=a_0 3^{1/2}/2^{3/2}$.

A. Frenkel model with constant interplanar separation

The first step in the calculation is to ensure the consistency between the continuum and the atomistic approaches, that is to use in the continuum approach, constitutive laws deduced from the atomistic simulation. The crystal is constructed as a {111} plane stacking normal to the (Ox) direction, and first the interplanar distance is kept constant, equal to a_x (cf. geometry in Fig. 6). The {111} planes are sheared along the (Oy) direction (a $\langle 112\rangle$-type direction), according to the homogeneous strain: $\bar{\varepsilon}_{xy}=\bar{\varepsilon}=\frac{1}{2}(u_y/a_x)$, so as to displace a {111} plane by u_y with respect to the next one. The crystal energy variation per unit area W is calculated as a function of the applied shear $\bar{\varepsilon}_{xy}$, using the aluminum potential. This quantity is displayed in Fig. 7, where the asymmetry between the twinning and antitwinning senses of shear appears clearly. If one restricts to shears such that the relative displacement between neighboring planes is smaller than b_t in the twinning sense, with $b_t=b_{90°}=\frac{2}{3}a_y$ (respectively, $b_{at}=2b_t$ in the antitwinning sense), it is seen in Fig. 7 that W is very close to a sine function and can be written

$$W=-\frac{A}{2}\left[1-\cos\left(\frac{4\pi\bar{\varepsilon}_{xy}a_x}{b}\right)\right], \tag{4}$$

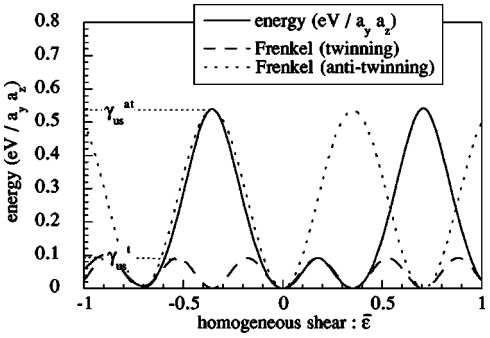

FIG. 7. Energy variation per unit area in {111} planes submitted to an homogeneous shear computed using the aluminum potential and comparison with the Frenkel model.

where b is set equal to b_t or b_{at} depending on the shear direction. The maximum A of the energy also depends on the shear direction. It must be remarked here that, although the cutoff distance in the aluminum potential is situated between the 10th and 11th neighbors, the interaction between {111} dense planes is essentially due to the nearest-neighbor planes, as ascertained for instance by the small difference between the intrinsic and extrinsic stacking fault energies, respectively, 156 and 144 mJ/m^2. Then, the crystal energy variation per unit area W obeys well the Frenkel form[15] and the maximum A can be assimilated to γ_{us}, the energy of the unstable fault as defined by Rice.[17] By considering that W varies linearly with the shear strain for small strains, one can show that $\gamma_{us}=\mu b^2/2\pi^2 a_x$.

B. Modulated interplanar separation

The interplanar distance a is now set to vary with x:

$$a(x)=a_x+e\cos\frac{2\pi x}{\lambda}=a_x+e\cos(kx), \tag{5}$$

a_x being the mean value of the separation, e being the magnitude of the modulation, λ is its wavelength, and k is its wave vector (Fig. 8). The {111} planes are submitted to the mean shear $\bar{\varepsilon}$ along the (Oy) direction; in this case, the displacement u_y is allowed to be no more homogeneous in the entire material, but depends on x, and locally the shear is $\varepsilon_{xy}(x)=\frac{1}{2}(\partial u_y/\partial x)$. The displacement u_y and the shear ε_{xy} are taken periodic, with period λ. The energy variation in a sample of thickness λ is now

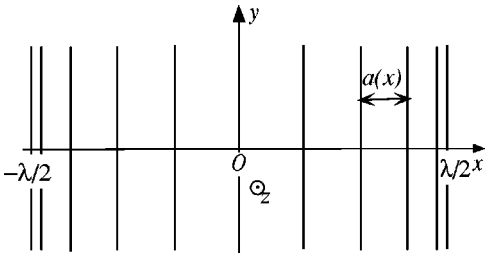

FIG. 8. Modulated separation between the {111} planes (the direction are the same as in Fig. 6).

$$W=-\int_0^\lambda \frac{\gamma_{us}(x)}{2}\left[1-\cos\left(\frac{4\pi\varepsilon_{xy}a_x}{b}\right)\right]dx$$

$$=-\int_0^\lambda \frac{\gamma_{us}(x)}{2}\left[1-\cos\left(\frac{2\pi a_x}{b}\frac{\partial u_y}{\partial x}\right)\right]dx. \tag{6}$$

As already seen, the unstable stacking fault energy is proportional to the shear modulus μ, which accounts for the {111} planes shear resistance. Now, the shear modulus depends on the {111} planes separation: the larger the plane separation, the smaller μ and the easier the shear; inversely, the more the planes are close, the more μ is important. According to theoretical approaches of the cohesive energy in materials,[20–22] it can be reasonably assumed that the shear modulus varies exponentially with the plane separation:

$$\mu=\mu_0\exp\left(-\frac{a(x)-a_x}{a_c}\right), \tag{7}$$

where μ_0 is the value of the shear modulus for the equilibrium distance a_x ($\mu_0=28.4$ GPa) and a_c is a characteristic length, equal to 0.3 Å with the potential used. According to Eq. (5): $[a(x)-a_x]/a_c=(e/a_c)\cos(2\pi x/\lambda)=\alpha\cos(2\pi x/\lambda)$, so that the energy 6 becomes

$$W=-B\int_0^\lambda \exp[-\alpha\cos(kx)]\left[1-\cos\left(\frac{4\pi\varepsilon_{xy}a_x}{b}\right)\right]dx, \tag{8}$$

B being a positive constant.

C. Determination of the local shear

In order to determine the local shear $\varepsilon_{xy}(x)$ which minimizes the energy, we apply a variational method: let $\varepsilon_0(x)$ be the shear that minimizes the energy. In Eq. (8), $\varepsilon_{xy}(x)$ is replaced by $\varepsilon_0(x)+\delta\varepsilon_{xy}(x)$, where $\delta\varepsilon_{xy}(x)$ is a perturbation of the solution, which corresponds to a displacement $\delta u_y(x)$. $\delta\varepsilon_{xy}(x)$ and $\delta u_y(x)$ are necessarily periodic with period λ. At first order in $\delta\varepsilon_{xy}(x)$, Eq. (8) becomes

$$W(\varepsilon_{xy})=W(\varepsilon_0+\delta\varepsilon_{xy})\approx W(\varepsilon_0)+\delta W$$

$$=W(\varepsilon_0)-B\int_0^\lambda \exp[-\alpha\cos(kx)]\frac{4\pi a_x}{b}$$

$$\times\sin\left(\frac{4\pi\varepsilon_{xy}a_x}{b}\right)\delta\varepsilon_{xy}dx. \tag{9}$$

Since $\delta u_y(x)$ is periodic with period λ, one has to solve

$$\delta W=0$$

and

$$\int_0^\lambda \delta\varepsilon_{xy}(x)dx=\int_0^\lambda \frac{1}{2}\delta\frac{\partial u_y}{\partial x}dx$$

$$=\frac{1}{2}[\delta u_y(\lambda)-\delta u_y(0)]=0. \tag{10}$$

These equations can be solved using the Lagrange multipliers method ($\delta W-\text{const}\int_0^\lambda\delta\varepsilon_{xy}\,dx=0$ for every $\delta\varepsilon_{xy}$), so that one obtains

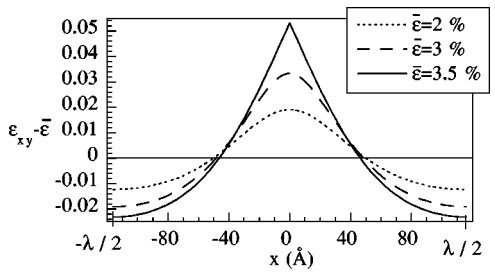

FIG. 9. Local shear versus x for different homogeneous applied shears $\bar{\varepsilon}$. $\lambda = 100a_x$ and $e = 0.1a_x$.

$$\exp[-\alpha\cos(kx)]\frac{4\pi a_x}{b}\sin\left(\frac{4\pi\varepsilon_{xy}a_x}{b}\right) = \text{const.} \quad (11)$$

The solution of Eq. (11) is

$$\varepsilon_{xy}(x) = \frac{b}{4\pi a_x}\arcsin[\exp(\alpha\cos(kx)+C)]. \quad (12)$$

C is a constant of integration which can be obtained numerically from the mean shear $\bar{\varepsilon}$, using

$$\int_0^{\lambda}\varepsilon_{xy}(x)dx = \lambda\bar{\varepsilon}. \quad (13)$$

According to Eq. (12), the constant C must be negative, smaller than $-\alpha$ in order for $\varepsilon_{xy}(x)$ to be defined for any x.

D. Analysis of the local shear

In Fig. 9, the local shear $\varepsilon_{xy}(x)$, defined by Eq. (12), is plotted for different mean strains $\bar{\varepsilon}$ in the twinning direction. As expected, $\varepsilon_{xy}(x)$ is maximum when the separation between planes is maximum, i.e., for $x=0$, and minimum when the separation is minimum, i.e., for $x=\pm\lambda/2$. For small mean strains $\bar{\varepsilon}$, the local shear $\varepsilon_{xy}(x)$ varies almost linearly with separation. As a matter of fact, for small $\bar{\varepsilon}$, $\varepsilon_{xy}(x)$ is small and if $\alpha = e/a_c$ is assumed to be small, one obtains

$$\begin{aligned}\varepsilon_{xy}(x)\frac{4\pi a_x}{b} &\approx \sin\left(\varepsilon_{xy}(x)\frac{4\pi a_x}{b}\right)\\ &= \exp(C-1)\exp(\alpha\cos(kx)+1)\\ &\approx \exp(C-1)[\alpha\cos(kx)+1]. \end{aligned} \quad (14)$$

Using Eq. (13) to determine C, we have then

$$\varepsilon_{xy}(x) \approx \bar{\varepsilon}[\alpha\cos(kx)+1]. \quad (15)$$

When $\bar{\varepsilon}$ is increased, nonlinear effects appear: in Fig. 9, it is seen that the shear becomes to localize in a nonuniform way, and for $\bar{\varepsilon} = \bar{\varepsilon}_c = 3.5\%$, an angular point appears at the maximum of shear. Above this value, C becomes larger than $-\alpha$ and the local shear $\varepsilon_{xy}(x)$ is no more defined for any x. For this critical value $\bar{\varepsilon}$, the limit of elasticity in the twinning direction is reached locally for $x=0$, since $\varepsilon_{xy}(0)+\bar{\varepsilon} = 5.25\% + 3.5\% = 8.75\% = \frac{1}{2}(b_t/4)/a_x$. In the antitwinning direction, the same features can be noted.

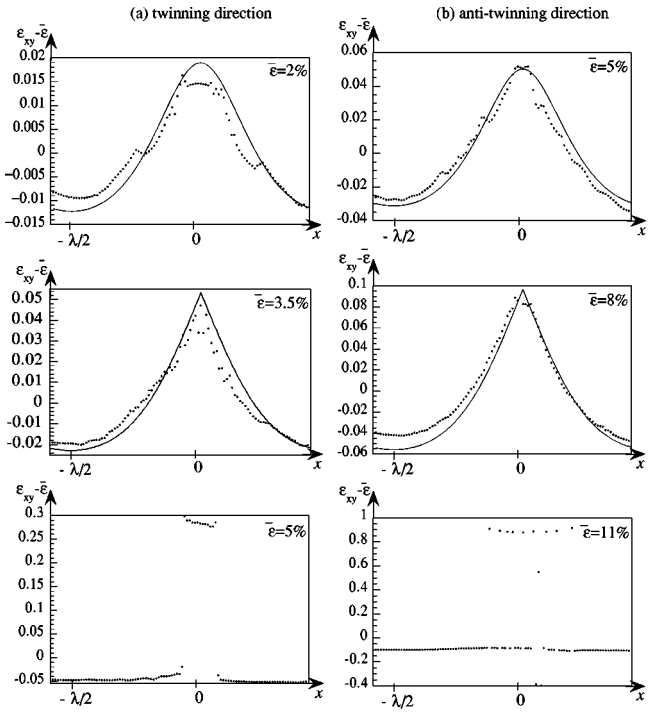

FIG. 10. Local shear versus x for different homogeneous applied shears $\bar{\varepsilon}$ in the twinning direction (a), and the antitwinning direction (b). On the first four figures, the solid line curves are determined from Eq. (12). The points result from the atomistic calculation.

E. Atomistic calculation and comparison to the analytical model

We have performed a simulation with the potential presented in Sec. II for aluminum. The structure studied is that presented in Fig. 6, with $\{111\}$ planes parallel to (Oyz). The crystal sample analyzed is representative of the bulk: in the (Ox) direction, two margins sufficiently large are chosen, while in the (Oy) and (Oz) directions, periodic boundary conditions are imposed. The interplanar separation of $\{111\}$ planes is modulated according to Eq. (5), with a wavelength equal to $100a_x$ and a magnitude e equal to $0.1a_x$. The crystal is then submitted to a homogeneous strain $\overline{\varepsilon_{xy}} = \bar{\varepsilon}$ and the atoms are allowed to move along the (Oy) direction so as to minimize the system internal energy. The displacement u_y of each plane indexed i with respect to its initial position (crystal submitted to the homogeneous strain) is thus calculated and the local shear is then determined: $\varepsilon_{xy}(i) - \bar{\varepsilon} = \frac{1}{2}[u_y(i) - u_y(i-1)]/a_x$. The values of $\varepsilon_{xy} - \bar{\varepsilon}$ obtained in the simulation are plotted in Fig. 10, together with the analytical solution given by Eq. (12).

In Fig. 10, one can see that the atomistic simulation results are in good agreement with the analytical analysis. When the homogeneous strain becomes larger than $\bar{\varepsilon}_c = 5\%$ (respectively, 11%) in the twinning (respectively, antitwinning) direction, for the $\{111\}$ planes close to $x=0$ Å (i.e., the planes for which the interplanar distance is maximum), the local shear strain reaches 30% (respectively, 80%), which corresponds to a displacement u_y of the order of b_t (respectively, b_{at}): neighboring planes have undergone relative displacements equal to those produced by the passage of dislocations.

V. CONCLUSION

The aim of this paper was to analyze the possible origins of the localized shear observed before dislocation nucleation at a surface step. Indeed, in a previous computer simulation of dislocation nucleation from a surface step in a stressed solid,[12] it has been shown that the transformation of the surface step into a real dislocation proceeds through the formation of a shear of increasing amplitude and extension, confined into a single dense plane in zone with the surface step, i.e., the plane where the nucleation will be activated for a sufficient applied stress. The maximum value attained by the localized shear, just before dislocation nucleation, corresponds to a displacement equal to $\mathbf{b}_{90°}/4$, which in the Frenkel model represents the point where the crystal becomes unstable, i.e., the elastic limit.

This shear localization has been related to the local stress field in the step region. Using the point force model as a first approach, we show that although the stress concentration does not involve any shear in the plane in zone with the step, it can influence indirectly the appearance of the localized shear by increasing the interplanar distance around the plane where this shear is observed. The interplanar distance increase can make shear easier in this plane. It is worth noting that the intensity of the point force, and consequently the change in interplanar separation, increases linearly with the step height h. If the step height is increased, one can then expect a decrease in the critical stress for dislocation emission. This point will be investigated in detail in complementary studies.

An analytical calculation based on the Frenkel model shows that the wider the planes are separated, the larger the local shear. For small strains, the localized shear determined from the analytical model varies almost linearly with the interplanar separation. But when the mean strain is increased, the local shear no longer varies linearly with the interplanar distance, and concentrates rapidly. Once again, the limit of stability is found to correspond to a displacement equal to $\mathbf{b}_{90°}/4$.

A variation in the interplanar distance, as produced here by the stress concentration in the vicinity of the step, will affect not only the dislocation nucleation from a surface step, but is also likely to take a part in many other problems, such as dislocation motion and Peierls stress, interaction between dislocations themselves, and with other defects, etc. Useful simulations are envisaged on these points.

The calculation presented here gives information on the barrier that a straight dislocation has to overcome to enter into the crystal: what is determined is the applied stress at which the system constituted of an infinite straight step on a surface becomes unstable and transforms into an infinite straight dislocation having sheared the crystal. In reality, the process of dislocation nucleation from a surface step is thermally activated: when the crystal is submitted to an external stress, there exists a minimum distance from the surface beyond which a dislocation formed from the step has a lower energy than the surface step. The energy barrier between the two states can be overcome by thermal activation and the saddle-point configuration is something like a dislocation half-loop emanating locally from the surface step. The determination of the energy of this half-loop requires a three-dimensional simulation able to determine out-of-equilibrium states such as saddle points. Of course the stress level at which thermally activated nucleation becomes possible is much lower than the stress level determined here in our two-dimensional (2D) calculation which corresponds to the complete disappearance of the energy barrier. The nucleation stress found here in the two-dimensional simulation is then an upper bound. Full 3D calculations would then be able to give information on the saddle energy and configuration inaccessible to the present 2D study.

*Electronic address: Sandrine.Brochard@lmp.univ-poitiers.fr

[1] J. Vanhellemont, C. Claeys, and J. Van Landuyt, Phys. Status Solidi A **150**, 497 (1995).
[2] A.G. Cullis, A.J. Pidduck, and M.T. Emeny, J. Cryst. Growth **158**, 15 (1996).
[3] S.V. Kamat and J.P. Hirth, J. Appl. Phys. **67**, 6844 (1990).
[4] K.J. Jagannadham and J. Narayan, J. Electron. Mater. **20**, 767 (1991).
[5] K.J. Jagannadham and J. Narayan, Mater. Sci. Eng., B **8**, 107 (1991).
[6] H. Gao, J. Mech. Phys. Solids **42**, 741 (1994).
[7] G.E. Beltz and L.B. Freund, in *Thin Films: Stresses and Mechanical Properties V*, edited by S. P. Baker *et al.*, MRS Symposia Proceedings No. 356 (Materials Research Society, Pittsburgh, 1995), p. 93.
[8] J. Zou and J.H. Cockayne, J. Appl. Phys. **79**, 7632 (1996).
[9] D.E. Jesson, S.J. Pennycook, J.M. Baribeau, and D.C. Houghton, Phys. Rev. Lett. **71**, 1744 (1993).
[10] J. Grilhé, Europhys. Lett. **23**, 141 (1993).
[11] L. Dong, A.J. Schnitker, R.W. Smith, and D.J. Srolovitz, J. Appl. Phys. **83**, 217 (1998).
[12] S. Brochard, P. Beauchamp, and J. Grilhé, Philos. Mag. A **80**, 503 (2000).
[13] D.M. Marsh, *Fracture of Solids*, edited by D. C. Drucker and I. J. Gilman (Interscience, London, 1963), p. 119.
[14] E. Smith, Int. J. Eng. Sci. **6**, 9 (1968).
[15] J. Frenkel, Z. Phys. **37**, 572 (1926).
[16] A. Aslanides and V. Pontikis, Comput. Mater. Sci. **10**, 401 (1998).
[17] J.R. Rice, J. Mech. Phys. Solids **40**, 239 (1992).
[18] J. Boussinesq, *Application des Potentiels à l'Étude de l'Équilibre et du Mouvement des Solides Élastiques* (Gauthier-Villars, Paris, 1885).
[19] S. Timoshenko and J.N. Goodier, *Theory of Elasticity*, 2nd ed. (McGraw-Hill, New York, 1961).
[20] Y. Sun, G.E. Beltz, and J.R. Rice, Mater. Sci. Eng., A **170**, 67 (1993).
[21] A. Blandin, J. Friedel, and G. Saada, J. Phys. (Paris), Colloq. **27**, C3-28 (1966).
[22] J.H. Rose, J. Ferrante, and J.R. Smith, Phys. Rev. Lett. **47**, 675 (1981).